PHOTOEVAPORATION OF COSMOLOGICAL MINIHALOS

BY THE FIRST STARS

by

Thomas Oscar McConkie

A senior thesis submitted to the faculty of

Brigham Young University

in partial fulfillment of the requirements for the degree of

Bachelor of Science

Department of Physics and Astronomy

Brigham Young University

August 2010

BRIGHAM YOUNG UNIVERSITY

DEPARTMENT APPROVAL

of a senior thesis submitted by

Thomas Oscar McConkie

This thesis has been reviewed by the research advisor, research coordinator, and department chair and has been found to be satisfactory.

Date	David Neilsen, Advisor

Date	Eric Hintz, Research Coordinator

Date	Ross L. Spencer, Chair

ABSTRACT

PHOTOEVAPORATION OF COSMOLOGICAL MINIHALOS

BY THE FIRST STARS

Thomas Oscar McConkie

Department of Physics and Astronomy

Bachelor of Science

Whalen et al. [1] conducted a survey which analyzed the effect of radiative feedback by one primordial star on subsequent star formation. Their study found results deviating from previous one-dimensional modeling. We extended the survey by performing two-dimensional simulations of cosmological mini-halo evaporation using the astrophysical fluid hydrodynamic code ZEUS-MP. This code was run varying primordial star size (25 - 80 $M_\odot$), halo to star distance (150 - 1000 pc), and halo central density(1.43 - 1569 cm^{-3}). We find that the ionization front of the star penetrates nearby halos to varying degrees according to their central density and proximity to the star. The degree of penetration may prevent, postpone, delay or have no effect on star formation.

ACKNOWLEDGMENTS

Contents

List of Figures

Chapter 1

Introduction

Several lines of observational evidence indicate that the universe is 74% dark energy, 22% dark matter, and 4% baryonic matter by content [2–6]. Just after the Big Bang and inflation, the universe was hot, ionized, and mostly featureless [2, 7–10]. As the universe expanded it cooled, allowing neutral atoms to form by redshift z of $\sim$ 1300 (or $\sim$ 400,000 yr after the Big Bang). At this point dark matter uniformly filled the universe except for slight dimples imprinted by gaussian fluctuations in quantum fields. These dark matter overdensities deepened as gravity drew more material into them, eventually collapsing into a vast web of filaments, sheets, and halos on gigaparsec scales [2,7–12]. Larger dark matter halos, or spheroidal clumps of dark matter and bound primordial H and He gas (baryons), formed out of gravitational mergers between smaller ones. This process gave birth to the cosmic network of galaxies and clusters (Figure1.1) discovered by deep field surveys like the Two Degree Field Galaxy Redshift Survey (2dF) and the Sloan Digital Sky Survey (SDSS) [13–15]. The gravitational dynamics of the early universe were governed by dark matter because it was much more abundant than primordial gas. Hydrogen and helium gas pooled in dark matter halos, setting the stage for first star formation.
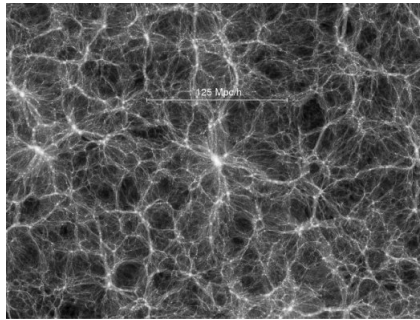
Figure 1.1 The formation of the first star-forming halo in the Universe. Lighter regions represent higher densities.

1.1 Formation of the First Stars

By $z \sim 20$–30 (100–200 million years after the Big Bang) some small halos, or minihalos, reached masses of $\sim 10^6$ solar masses ($M_\odot$), achieving central baryon densities that enabled gas in them to cool and collapse into the first stars. As primordial gas contracted in the core of the halo, the bulk inflow motion of atoms from higher altitudes became randomized disordered motion, or heat, upon collision near the center. This happens because mean free paths decrease in the core as density rises and because infalling gas reaching the center has nowhere to go. As the central gas heats, it achieves an equilibrium between inward gravitational forces and outward thermal pressures that support it against further collapse. The equilibrium persists until some mechanism transports heat from the halo core. In star-forming clouds today, dust grains radiate infrared (IR) photons that carry heat out of the core, allowing further collapse of the gas into a star. In the pristine gas of high-redshift minihalos below 10^8 $M_\odot$, only molecular hydrogen can cool the gas. Molecular hydrogen forms in these halos through two gas-phase reactions:

$$H + e^- \rightarrow H^- + \gamma \qquad H^- + H \rightarrow H_2 + e^- \tag{1.1}$$

$$H^+ + H \rightarrow H_2{}^+ + \gamma \qquad H_2{}^+ + H \rightarrow H_2 + H^+. \qquad (1.2)$$
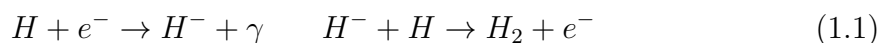
The H_2 molecule has vibrational and rotational modes that can be excited through collisions with the H, He, and free electrons. These modes eventually relax, emitting an IR photon which can escape the cloud and allow gravity to collapse the baryons in the core of the halo into a primordial star. H_2 is a relatively inefficient coolant in comparison to dust, and its low cooling rates lead to very large accretion rates onto protostars, resulting in very massive primordial stars, 30–500 $M_\odot$ [16–22]. Primordial stars predated the first galaxies by several hundred million years and formed in isolation (one per halo). With surface temperatures exceeding 100,000 K, their luminosities were millions of times greater than the sun, making them intense sources of both ionizing ultraviolet (UV) radiation ($h\nu > 13.6$ eV) and Lyman-Werner (LW) H_2 photodissociating photons (11.18–13.6 eV). Population III (or Pop III) stars had relatively short lifetimes of 2–3 Myr [23].

1.2   UV Breakout from the First Stars

When one star lights up in a cluster of halos, its ionizing UV is not free to stream unimpeded into the intergalactic medium (IGM). H and He in the hosting star halo is opaque to photons with less than 13.6 eV. Ionizing UV radiation emerges from the star behind an abrupt wall of radiation known as an ionization front (I-front). The ionized gas bounded by the I-front is called the H II region, which can be $20,000$–$30,000$ K and has only $\sim$ one neutral atom in $\sim 10^6$. Close to the star, where flux is intense, the I-front propagates supersonically with respect to the gas through which it travels, leaving it essentially undisturbed in its wake. This is an R-type front. As the H II region grows, the I-front slows down and becomes D-type, pushing a dense shell

of shocked neutral gas before it. When a star enters the main sequence, its ionizing UV radiation breaks out of the halo on time scales of 100 kyr, propagating into the IGM as an R-type front. This radiation front engulfs nearby halos and begins to photoionize and photoevaporate them, impacting star formation.

As discussed earlier, these first stars also emitted an intense flux of UV photons in the LW band (11.18–13.6 eV). These photons cannot ionize H or He but do photodissociate H_2, the key coolant responsible for Pop III star formation. Because their energies lie below the ionizing limit of H and He, LW photons reach nearby halos before the I-front, postponing star formation in them by partly sterilizing them of H_2. The photons that are not absorbed by H_2 propagate to great distances in the IGM due to the transparency of H and He in this band. These photons build up a background flux in the IGM over time.

1.3   Impact of Pop III Stars on Their Environment

Cosmological minihalos often form in clusters, an effect known as cluster bias. The influence one massive star has on star formation in neighboring halos is key to the rise of the first stellar populations. This is known as *radiative feedback*: it is positive if nearby star formation is promoted and negative if it is suppressed. Local radiative feedback by one star on other halos within a cluster has come into better focus over the past 10 years in a series of numerical studies. Models fall into two categories: numerical simulations in cosmological boxes that capture early structure formation but must approximate early UV fields as uniform backgrounds (no transport) [24–31], and detailed radiation hydrodynamical models that follow the photoevaporation of a single halo in good detail but not its eventual collapse into a star [1,32–34]. The early studies in large computational boxes generally found that ionizing and LW photons

delay but do not completely suppress star formation in halos. The halos simply grew to larger masses until their cores were sufficiently shielded from radiation to collapse into a star. Later, more detailed models of the radiation hydrodynamical evaporation of individual halos revealed more complex possibilities. In particular, they demonstrated that ionizing UV photons couple strongly to primordial chemistry, strongly altering halo evolution. The most physically complete calculations of minihalo photoevaporation by a nearby star performed to date reveal that it proceeds in several stages:

- Partial or complete LW photodissociation of the halo prior to the arrival of ionizing photons. This does not disrupt the halo but can delay or halt the collapse of the core by reducing H_2 cooling.

- Transition of the incoming I-front from R-type to D-type along lines of sight near the center of the halo along its axis. This causes the I-front to assume a cometary appearance, with the central regions of the halo casting a shadow. A dense shell of gas is driven inward toward the core of the halo.

- The formation of an H_2 layer in the outer regions of the front. Since I-fronts are not complete discontinuities there is some distance in between the ionized gas and the neutral gas. In this region, high energy photons penetrate and "pre-ionize" the gas, creating excellent conditions for the formation of H_2 [35]. This layer of H_2 partially shields the halo from further LW bombardment, in some cases even allowing H_2 to reconstitute in the halo core [29, 36].

- The star dies. The H II region begins to cool out of equilibrium, which means its temperature falls faster than its ionization fraction. H_2 forms explosively in ionized fractions of $\sim 10\%$ and temperatures near a few thousand K. Residual pressure in the cooling relic H II region continues to wrap cylindrically around

the partially photoevaporated halo, compressing it from behind, while the momentum of the shocked dense shell carries gas heavily enriched with H_2 into the core of the halo.

Whalen et al (2008) found four possible outcomes for star formation in the halo. If the halo is sufficiently dense, there may be no disturbance to the core and star formation proceeds uninterrupted. On the other hand, diffuse halos are completely destroyed either by R-type fronts that flash-ionize the cloud or by D-type fronts that snowplow gas from the core. At intermediate central densities, the relic H II region shock compresses the core to higher densities and enriches it with H_2. Since the H II region has a much higher temperature than the neutral gas within the halo and the shadow behind it, the gas in the halo is compressed from multiple directions. This compression raises central densities faster than if the halo is left to evolve on its own, accelerating its cooling and collapse into a new star. This is known as accelerated collapse. If the relic H II region shock compression is too strong it severely disrupts the core, delaying or altogether preventing star formation [1].

1.4 Overview

Several parameters govern radiative feedback between first-generation minihalos. Some examples are the mass and distance of the star, the mass and central density n_c of the neighbor halo, the temperature of the star (and hence spectral profile and ratio of LW to ionizing photons), and the lifetime of the star. Whalen et al (2008) studied minihalo photoevaporation, by a 120 $M_\odot$ star at 4 different stages of collapse. However, the effects of low-mass primordial stars on nearby halos are yet to be evaluated. We extend the survey of Whalen et al (2008) by computing a grid of models in which a star-forming minihalo is photoevaporated by 25, 40, 60, and 80 $M_\odot$ stars. We as-

sess the survival of star formation in each of these cases and derive general rules for local radiative feedback for use in both analytical models and numerical simulations of high-redshift structure formation. In § 2 we describe our numerical methods and models and in § 3 we discuss our results, concluding in § 4.

Chapter 2

Numerical Algorithm and Problem Setup

2.1 ZEUS-MP Astrophysical Fluid Hydrodynamics Code

Our numerical algorithm is a modified version of the ZEUS-MP astrophysical fluid hydrodynamics code, which was developed at the University of Illinois at Urbana-Champaign (UIUC) and the University of California, San Diego (UCSD) [37]. This algorithm finite differences Euler's equations of fluid dynamics:

$$\frac{\partial \rho}{\partial t} = -\nabla \cdot (\rho \mathbf{v}), \tag{2.1}$$

$$\frac{\partial \rho v_i}{\partial t} = -\nabla \cdot (\rho v_i \mathbf{v}) - \nabla p - \rho \nabla \Phi - \nabla \cdot \mathbf{Q}, \tag{2.2}$$

$$\frac{\partial e}{\partial t} = -\nabla \cdot (e\mathbf{v}) - p\nabla \cdot \mathbf{v} - \mathbf{Q} : \nabla \mathbf{v}, \tag{2.3}$$

where ρ, e, and v_i, are the mass density, internal energy density, and velocity components, respectively, and $p = (\gamma - 1)e$ and $\mathbf{Q}$ are the gas pressure and von Neumann-Richmeyer artificial viscosity. These equations describe mass, momentum, and energy conservation in the fluid, respectively. To evolve the left hand side of each equation, ZEUS-MP uses operator splitting, in which the fluid variable is evolved by each term on the right hand side sequentially, with terms in consequent updates incorporating the partially evolved fluid variable of the previous update. The divergence terms describe changes in a flow variable at a mesh point due to material carried into the point from upstream, which is known as *advection*. They are evaluated in the ZEUS-MP advection, or transport routines. The other terms describe changes to ρ, e, and $\mathbf{v}$ by forces exerted on the flow from outside the mesh point. They are evaluated in the ZEUS-MP source routines. ZEUS-MP can solve these equations in one, two, or three dimensions on spherical, cylindrical, or cartesian coordinate meshes.

2.2   Primordial Chemistry/Radiative Transfer

Our simulations incorporate a 9-species reaction network for H, H^+, He, He^+, He^{2+}, H^-, H_2^+, H_2, and e^-, photon-conserving UV radiative transfer, and multispecies flow hydrodynamics. Although more than 300 reactions can occur in primordial H and He gas, only the thirty most important to the formation and destruction of H_2 are included in the network. We follow the flow and chemistry of these species with 9 additional continuity equations and the non-equilibrium rate equations of Anninos et al (1997) [38, 39]:

$$\frac{\partial \rho_i}{\partial t} = -\nabla \cdot (\rho \mathbf{v}) + \sum_j \sum_k \beta_{jk}(T)\rho_j\rho_k + \sum_j \kappa_j \rho_j. \qquad (2.4)$$

Here, κ_j is the photoionization rate coefficient of the species ρ_j, and β_{jk} is the reaction rate coefficient that describes the production (+) or loss (-) of species i by species

j and k. The divergence terms are evolved in the advection routines, the reaction network is updated in the chemistry routine, and the photoionization rate coefficient is computed in the radiative transfer routine.

ZEUS-MP can transport UV photons from a point source at the center of a spherical mesh (RTP), in plane waves along the z-axis in a cylindrical grid (ZRP) or along the x-axis of a cartesian box (XYZ). On an RTP grid, photons propagate along rays that extend from the point source out to the outer boundary, piercing every intervening cell. In XYZ or ZRP boxes, plane waves are propagated along rays parallel to the x and z axes respectively. Each ray originates from a cell on the lower boundary and extends to the opposite cell on the upper boundary. Along a given ray the equation of radiative transfer is solved to compute the rate coefficients κ_j in each cell that appear in the reaction network shown above. The equation of transfer is [40]:

$$\frac{1}{c}\frac{\partial I_\nu}{\partial t} + \hat{\mathbf{n}} \cdot \nabla I_\nu = \eta_\nu - \chi_\nu I_\nu, \tag{2.5}$$

where η_ν, χ_ν, and c are the emission coefficient, the absorption coefficient, and the speed of light respectively. Equation 2.5 can be simplified by a series of logical approximations to obtain the static approximation of radiative transfer:

$$\hat{\mathbf{n}} \cdot \nabla I_\nu = -\chi_\nu I_\nu, \tag{2.6}$$

in which I(t,$\mathbf{x}$,$\hat{\mathbf{n}}$,ν) is the specific intensity of the radiation field at the position $\mathbf{x}$ approached from the direction $\hat{\mathbf{n}}$. This approximation allows us to dispense with the time derivative which would reduce computation to time steps that are much smaller than necessary for accuracy.

2.3   Energy Equation

We perform operator-split updates to the gas energy due to photoionizational heating and cooling:

$$\dot{e}_{gas} = \Gamma - \Lambda. \tag{2.7}$$

Here, Γ represents the photoheating rate and Λ represents the sum of six cooling rates: electron collisional and ionizational cooling, recombinational cooling, H_2 cooling, bremsstrahlung cooling, and inverse Compton cooling. In electron-atom collisions the electron can either excite the atom, which emits a photon upon de-excitation, or it can remove an electron from the atom. In either case, kinetic energy is lost from the original electron, which cools the gas. In recombinations, an ion captures an electron, removing it and its energy its energy from the gas, reducing its temperature. In bremsstrahlung cooling, free electrons in a gas are deflected by the positive nuclei of ions and they emit photons to conserve momentum and kinetic energy. In doing so, the electron slows down and the gas is cooled. Radiation by H_2 through ro-vibrational modes was discussed earlier. Compton cooling occurs as free electrons impart energy to high redshift photons in the comic microwave background (CMB) via inverse Compton scattering; this process becomes more prominent with redshift.

2.4   Time Step Control

The differential equations governing the evolution of hydrodynamics, radiative transfer, and chemistry each have highly disparate characteristic time scales. To avoid restricting the entire algorithm to unnecessarily small time steps, we adopted an adaptive hierarchal update scheme. At the beginning of a given timestep in a run we first advance each species' mass fraction and the gas energy density by the minimum

of the chemistry time

$$t_{chem} = \frac{n_e}{\dot{n}_e} \qquad (2.8)$$

and the photoheating time

$$t_{heat} = \frac{e_{gas}}{\dot{e}_{heat/cool}}. \qquad (2.9)$$

We repeat these updates until the smaller of the photoheating and Courant times is reached, at which point full hydrodynamical updates of ρ, e, and $\mathbf{v}$ are performed. We use the new species mass fractions from a given reaction network update in subsequent radiative transfer and gas energy solves. Global solution concurrency is enforced by using the grid minimum at each stage so that the solution in one region of the grid does not outpace the others.

2.5   Problem Setup/Initial Conditions

We use a two-dimensional axisymmetric cylindrical coordinate (ZR) grid with 1000 zones in z and 500 in r. The mesh boundaries were -125 pc and 125 pc in z and 0.01 pc and 125 pc in r, giving a spatial resolution of 0.25 pc. Outflow conditions were applied at the upper and lower boundaries in z and the outer boundary in r. Reflecting conditions were imposed at the inner r boundary. The halos were centered on the z axis, with only the upper hemisphere on the grid. The 1.35×10^5 M$_\odot$ halos we used were computed from cosmological initial conditions in the Enzo AMR code [41]. Four evolutionary stages of this halo were studied, with central densities that increased with decreasing redshift. Dark matter gravity was included by adding in a separate potential that completely canceled out the pressure forces everywhere on the grid and holding it fixed for the duration of the simulation. Force updates to gas velocities were calculated with this potential every hydrodynamical time step. Since at $z \sim 20$ merger times were approximately 20 Myr, ignoring dark matter dynamics

causes few errors because our simulations are only run for 10 Myr. Updates to the self gravity of the gas were performed every hydrodynamical time step by solving Poisson's equation with a two-dimensional conjugate gradient (CG) solver. The gas in our halos was 76% H and 24% He by mass. We assumed ionized and H_2 fractions of 1.0×10^{-4} and 2.0×10^{-6}, respectively, which are consistent with the free electron fractions expected at $z \sim 20$.
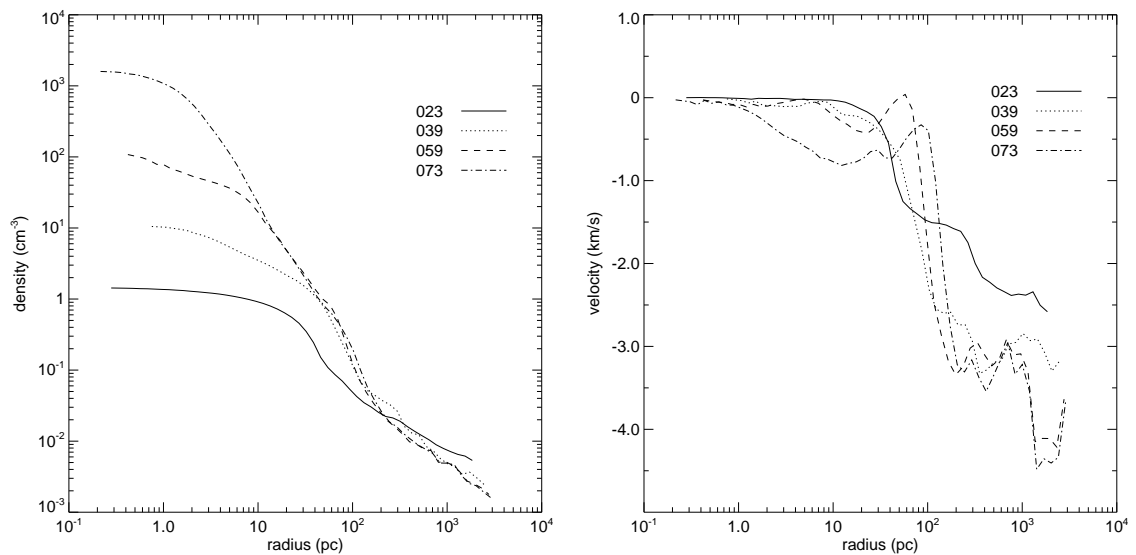
Figure 2.1 Spherically-averaged baryon profiles for the 1.35×10^5 M$_\odot$ halo at four stages of evolution. The redshifts of the 023, 039, 059, and 073 profiles are 23.9, 17.7, 15.6, and 15.0, respectively, with corresponding central densities of 1.43, 10.5, 108, and 1596 cm^{-3}. Left: densities. Right: radial velocities.

The four evolutionary stages of the halo we considered had initial central densities of 1.43, 10.5, 108, and 1569 cm^{-3} (hereafter 023, 039, 059, and 073 respectively). Each was illuminated by 25, 40, 60, and 80 M$_\odot$ stars at distances of 150, 250, 500,and 1000 pc for their respective life times of 6.46, 3.86, 3.46, and 3.01 Myr [23], a total of 64 models. Although each model is evolved for 10 Myr, the radiation in the simulation was only on for the lifetime of the star. This radiation was assumed to be a blackbody spectrum. The blackbody spectrum was discretized into 40 bins uniformly spaced in

energy from 0.255–13.6 eV and 80 logarithmically spaced bins from 13.6–80 eV.

Chapter 3

Results and Discussion

The Whalen et al 2008 [1] study revealed four final fates for star formation in cosmological halos near a primordial star. Complete destruction of the halo occurs if the approaching I-front sweeps through the halo and snowplows the majority of the gas out of the dark matter potential making the halo sterile to star formation. Very diffuse halos, with $n_c < 1$ cm^{-3} were victim to this event. If the center of the halo was dense enough, $n_c > 100$ cm^{-3}, it was shielded from LW photons and star formation proceeded with out interruption. Star formation is delayed when the core of the halo is exposed to a high flux of LW photons, which dissociate the H$_2$ and cause the star to form later than it would have had the neighboring star not been present. Accelerated star formation can occur when H$_2$ formed in the I-front merges with the core and the I-front wraps around the core and compresses the gas. Both of the latter occur for stars with medium central density. We will compare our 25 - 80 M$_\odot$models, which are evolved 10 Myr, to the 120 M$_\odot$model by Whalen et al. (2008) [1] run out to the same time. The summary of that survey can be seen in Figure 3.1.
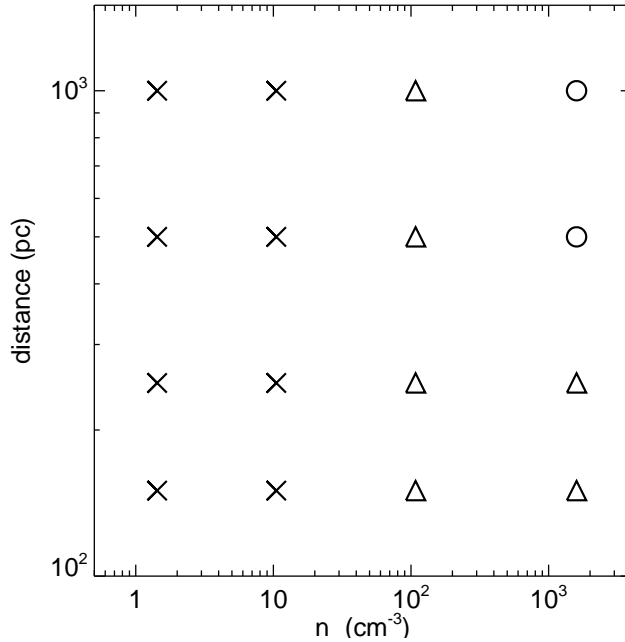
Figure 3.1 Star formation in a 1.35×10^5 M$_\odot$halo in the vicinity of a 120 M$_\odot$star, from [36]. The central baryon densities n_c of the halo at the time of illumination were 1.43, 10.5, 108, and 1596 cm^{-1}, respectively. The 120 M$_\odot$star was at 150, 250, 500 and 1000 pc. Completely evaporated halos with no star formation are labeled by crosses and halos with delayed or undisturbed star formation are represented by triangles and circles, respectively.

3.1   25 - 80 M$_\odot$ Stars

Figures 3.2 and 3.3 summarize the effects of local ionizing and LW radiation on star formation near 25, 40, 60, 80 M$_\odot$stars. First, we note first that in each of these stars new star formation obeys the same trends as the 125 M$_\odot$. This being, suppressed, then delayed , and eventually unaffected as the central baryon density and star distance grow. These tends are attributed mainly to the I-front shock momentum as it reaches the halo core. In review, delayed star formation is due to either disruption of the center of the halo by the relic I-front shock, LW photodissociation of the core of the

halo, or both. Unaffected star formation occurs if the halo core is completely shielded from the LW flux, this also guarantees that the relic I-front shock will not reach the core before the star forms. In the 60 and 80 M$_\odot$ tables we have drawn a line from the upper left to the lower right marking the boundary between quenched star formation and delayed or undisturbed formation (corresponding lines for 25 and 40 M$_\odot$ stars are not shown due to their violent deaths by Super Nova explosions whose kinetic feedback must also be considered and is beyond the scope of this paper). The death of the stars just below the lines are usually unambiguous since the shock completely snow plows the baryons form the core. Just above the line we see dependance on the mass of the illuminating star. The line shifts up and the the right with increased neighboring star mass. However, from 25 - 80 M$_\odot$ the shift is quite small. For fixed distance and baryon density the star formation is at most delayed if once uninhibited, or prevented if delayed. The overall star formation remains unchanged above and below this band. Note that the lines are drawn to evenly divide the space between the symbols and should be taken as rough order of magnitude estimates.

The question is now posed as to why there is such uniformity in star formation given different neighbor star masses. This is due to the cooperation of flux intensity and star lifetime. First, low-mass Pop III stars have a dimmer flux which causes the front to transform from R to D-type further from the halo center. In Figure 3.4 panel (a) we have plotted the velocity profiles for the I-front the moment it becomes D-type in the $n_c = 180$ cm^{-3} halo 500 pc from 25 - 120 M$_\odot$ stars. In each profile the transition is marked by the forward peak, which is at 80, 75, 60, 55, 50 pc for the 25, 40, 60, 80, and 120 M$_\odot$ stars respectively. However, we must consider that lower mass stars are longer lived and therefore drive the I-front for longer times. This effect condenses the I-font penetration distance dispersion to 10 pc by the time the stars die, This is depicted in Figure 3.4 panel (b). For this halo, the I-fronts reach

the core with nearly the same velocity, which is well below the escape speed, with each star. Though we have only discussed one particular density and distance, this pattern actually holds for all halos where the I-front falls short of the core when the star dies, thus allowing a delayed or uninterrupted star formation. Returning to panel (a) of Figure 3.4 we note that the velocity profiles have split into two smaller peaks. This phenomena is due to penetration of hard UV photons into the dense shocked gas preceding the front. This drives a backflow into the shock. This feature is common in I-fronts due to hard UV photons and is discussed further in section 4.1 and Figure 17 of Iliev et al. (2009) [42]. The evolution in the spectral profile from 25 to 120 $M_\odot$, which causes ionized gas temperatures to rise by more than 50 % in the H II region, accounts for the variation in peak velocity in Figure 3.4. Had each I-front been driven by a monochromatic flux instead and had same magnitude and duration, the spread of the peaks in would have been less that 10 pc.

According to the Whalen et al. (2008a) [1] survey, formation of a new star depends mainly on the momentum imparted by the relic I-front shock to the core of the halo. In a few cases of our survey the compression of the shadow of the halo toward the axis also determines star formation. In our new models the halo forms a shadow on the same time scale as a 120 $M_\odot$ star but pressure from the surrounding relic H II region drives it inward toward the axis for up to twice the time before the star dies, squeezing a flow backward into the center of the halo. As shown in Figure 3.5 for halo 073 150 pc from a 60 $M_\odot$ star, this back flow can slightly displace the baryons from the halo center. This gas clump keeps it shape and has velocities well below the escape velocity of the halo. This small displacement at 10 Myr prevents the star from forming though it would have if only the relic I-front shock were present. These backflows were especially collimated in the axial symmetry assumed in our models, however we expect them to be present in three dimensional halos since the

are approximately spherical.

The halos in which uninterrupted star formation occurs, molecular hydrogen mass fractions rapidly rise from the starting value of 2×10^{-6} to 10^{-4} at star ignition, even with the LW flux, since the core shields itself. This is shown in Figure 3.6 on the right panel for the halo $n_c = 1596$ cm^{-3} 500 pc from 25, 40, 60, 80 $M_\odot$. The core collapses even as the outer layers of the halo are stripped away by supersonic outflows, and a star forms just as quickly as in the absence of radiation. Since we begin with cosmic mean H$_2$ fractions of 2×10^{-6} instead of more realistic values of 10^{-4} for simplicity we have established lower limits to self-shielding and cooling.

One difference the 120 $M_\odot$ models have from the others is the delayed star formation at 150 and 250 pc in the halo at $n_c = 108$ cm^{-3}, which does not occur near 25 - 80 $M_\odot$ stars. This happens because the shock remnant traverses the core of the halo sooner, allowing gas to later pool in the dark matter potential and reach its original density at the center by 10 Myr, as we show in the left panel of Figure 3.6 at 150 pc. This back fill allow new stars to form before 20 Myrs has elapsed. Similar behavior would be seen in low-mass runs evolved beyond 10 Myr but would most likely not result in a new star prior to severe disrupture by a merger. The solid lines in Figure 3.6 represent the higher densities at earlier times in the outer regions of the halo due to compression by the relic I-front shock as it envelops the halo.

We find that the higher ration of LW to ionizing photons of low-mass Pop III stars has no effect on nearby star formation. The lower fluxes of these stars offset their higher ratios, and in any event LW photons from a single star cannot prevent a new star from forming in a nearby halo prior to the appearance of the LW backgrounds at lower redshifts. They can only delay it for the life of the proximate star. Without LW photons halo collapse times at $n_c \sim 2000$ cm^3 are 7 - 10 Myr. At such densities, Whalen et al. (2008a) [1] find that the core begins to strongly self-shield from local

LW flux. If the core could collapse before the arrival of the I-front, its n_c would be far greater, be fully shielded from LW flux, and form a star anyway. Halos that are completely ionized are too diffuse to form a star before the I-front reaches the core even in the absence of LW photons. Cores that form a star after the death of a nearby star could not have created one sooner without LW flux because their star formation times are even greater than 7 Myr. Finally, halos that are too severely disrupted by the relic I-front shock to form a star cannot collapse prior to the arrival of the shock in the absence of LW radiation for the same reason. Thus, in none of these outcomes would a star have formed if there had been no LW flux. In the latter two cases, we find that H$_2$ fractions at the center of the halo reacquire their original values 100 - 200 kyr after the star dies and that cooling and collapse of the core begins anew, augmented in some cases by molecular hydrogen advected into it by the relic I-front shock. Any suppression or delay of star formation is entirely due to bulk flows driven into the core driven by relic I-front shock and shadow dynamics, not to the destruction of H2, which quickly reconstitutes in the core after the star dies. Thus, local ionizing UV flux governs new star formation in clustered halos, not local LW photons.

Exceptions of this occur when baryons are very close to the star, 25 - 150 pc. In these cases, when a star is irradiating a clump of baryons in the same halo, Hasgawa et al. (2009) find that clouds with freefall times that are shorter than ionization times can be prevented from collapsing by 25 M$_\odot$ stars because they have the highest LW ionizing photon ratio. This never occurs in our models because of the much lower LW fluxes at typical halo distances within the cluster, but such scenarios are quite relevant to the formation of Pop III binaries within a halo (Turk et al. 2009). Persistent LW backgrounds at lower redshifts can by themselves prevent secondary star formation in the cluster by not allowing partially evaporated cores to cool after the death of the star. However, the exclusion of radiation hydrodynamical effects in past studies may

have led them to overestimate this effect, as we discuss in § 4.

3.2   Ionization Front Instabilities

Longer illumination times and lower fluxes promote the onset of dynamical instabilities in the D-type ionization front as it engulfs the satellite halo, as we show for the 073 halo 150 pc away from a 25 $M_\odot$ primordial star in the left panel of Figure 3.7. They arise because the I-front assumes a cometary shape and because the high energy tail of the spectrum forms H_2 between the front and the dense shell that radiatively cools the shell [36, 43]. Using rigorous perturbation analysis, [44] discovered that D-type fronts driven by photons that are oblique to the front are always unstable, and that the growth rates of the modes rise with the angle of incidence of the photons. This, together with cooling of the shocked shell by H_2, is the origin of the instabilities in the I-front enveloping the halo in Figure 3.7. At early times, we find that the modes with the greatest amplitudes are indeed those furthest out along the arc of the I-front, where photons are incident to the front at the greatest angles. At intermediate and later times the perturbations grow nonlinearly and degenerate into turbulent fluid motion along the outer segments of the arc. The amplitudes of the modes closest to the axis of the halo are small and instabilities never puncture its core. Much more prominent perturbations have been found in planar I-fronts approaching spherical molecular cloud cores in numerical models with efficient radiative cooling by molecules [45]. These phenomena have been proposed for the origin of the "Pillars of Creation" in the Orion Nebula (see Figure 3.8), but they are different from those in our simulations. They begin as Vishniac thin-shell overstabilities [46] caused by efficient molecular cooling in plane-parallel I-fronts, not curved ones, and later erupt into violent instabilities driven by ionizing radiation. In the Mizuta et al. [45] models

the unstable modes do propagate into the molecular cloud core. This never occurs in our simulations because H_2 cooling is too inefficient to incite Vishniac modes.

We point out these features because they are prominent in many of our models, but they do not affect star formation in the halo because they never approach its inner regions. Mostly, they just roil gas along the shock, breaking it up into clumps that can persist for up to 10 Myr. We find that they appear when the star is 150 or 250 pc from the halo and are most prominent with 25 and 40 $M_\odot$ stars. Fewer instabilities appear as stellar mass increases; they arise in only two of the 120 $M_\odot$ models and have lower amplitudes. There are two reasons for this. First, higher mass stars have greater LW fluxes that lower H_2 cooling in the dense shell. Second, larger ionizing UV fluxes result in shorter-lived cometary profiles in which unstable modes can develop. The arc is crushed downward into the shadow of the halo more quickly and the instabilities have less time to develop.
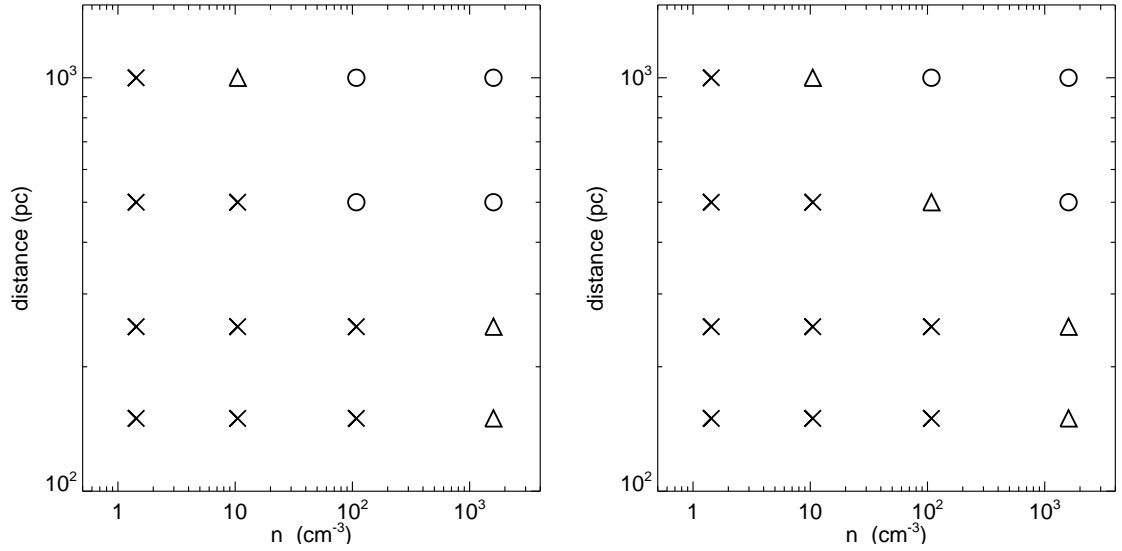
Figure 3.2 Star formation in the halo when illuminated by a 25 $M_\odot$ star (left) and a 40 $M_\odot$ star (right) at four central baryon densities n_c, 1.43, 10.5, 108, and 1596 cm^{-3}, and at four distances from the star, 150, 250, 500 and 1000 pc, which are typical interhalo spacings within a cluster. Completely evaporated halos with no star formation are labeled by crosses, and halos with delayed or undisturbed star formation are indicated by triangles and circles, respectively.
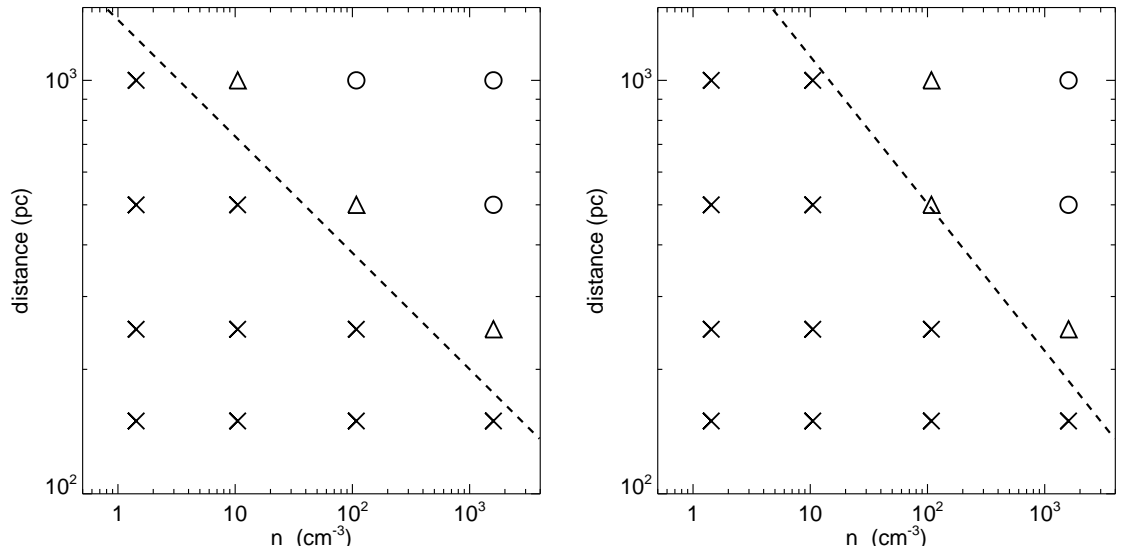
Figure 3.3 Star formation in the halo in the vicinity of a 60 $M_\odot$ star (left) and an 80 $M_\odot$ star (right) at the central gas densities and distances to the star considered in our study. Completely ionized halos with no star formation are labeled by crosses, and halos with delayed or undisturbed star formation are indicated by triangles and circles, respectively. The dotted lines mark the threshold for star formation in the evaporated halos, above which it proceeds and below which it is quenched.
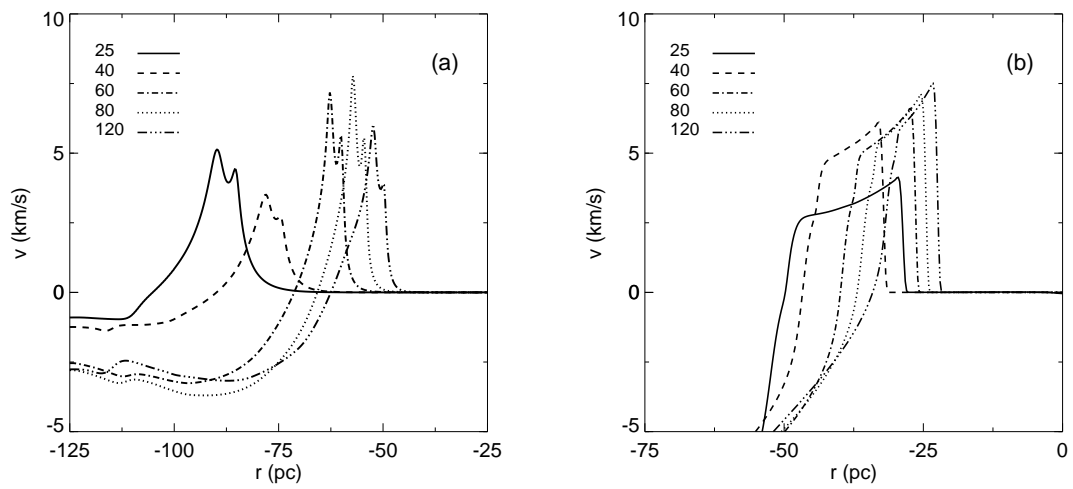
Figure 3.4 I-front gas velocity profiles through the central axis of the halo for 25, 40, 60, 80, and 120 $M_\odot$ stars 500 pc from halo 059 ($n_c = 108$ cm^{-3}). Panel (a): velocity at the time each front transforms from R-type to D-type. Panel (b): gas velocity profiles at the time each star dies.
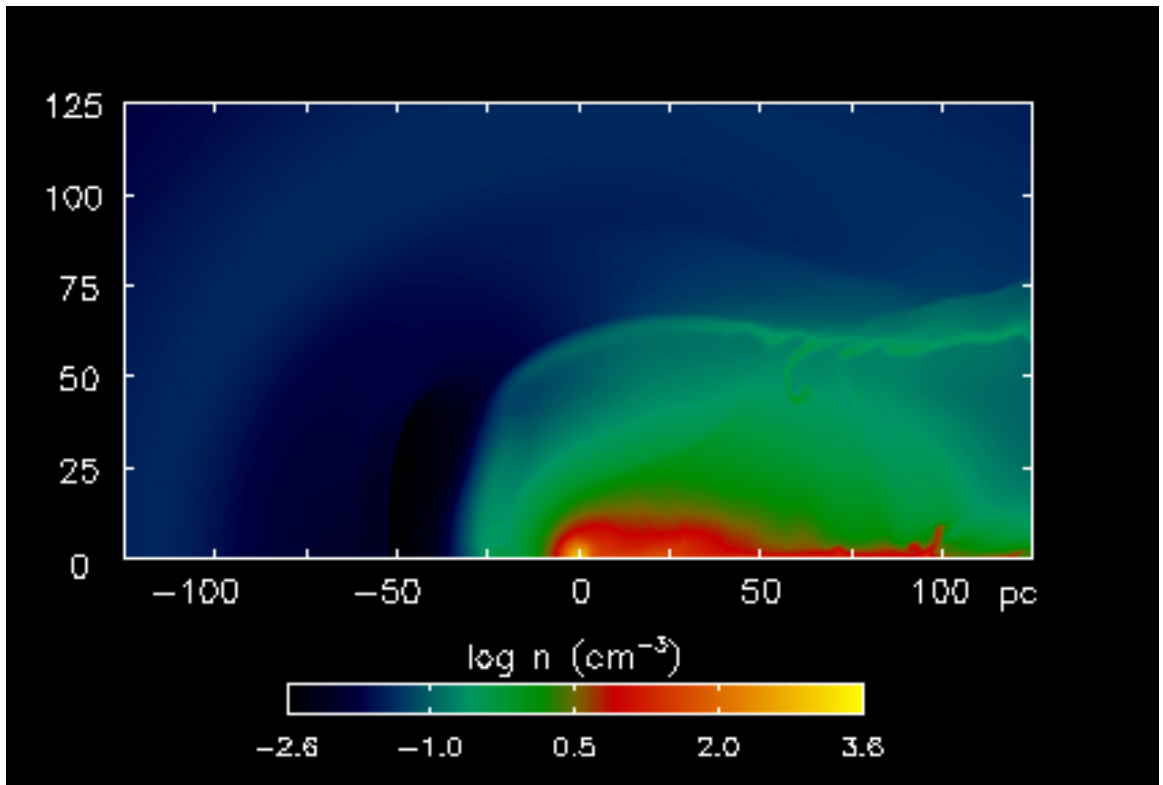
Figure 3.5 Evaporated halo with $n_c = 1596$ cm^{-3} (halo 073) 150 pc from a 60 M$_\odot$ star at 10 Myr. The core of the halo is slightly displaced to the left of center by backflow from the collapsed shadow on the right.
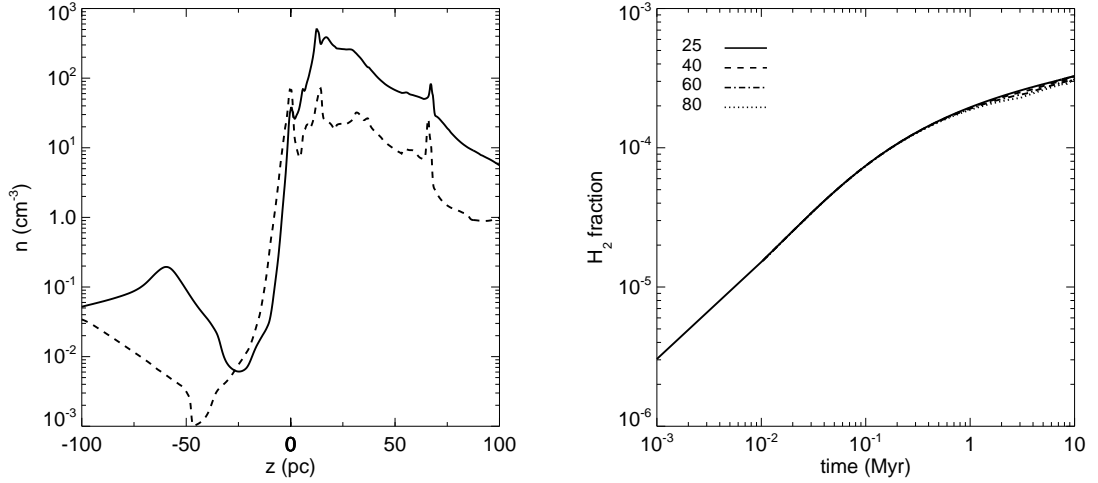
**Figure 3.6** Left panel: the flow of baryons back into the center of the dark matter potential from the relic H II region, as shown in these density profiles along the central axis of the halo. Solid: 5.5 Myr; dashed: 10 Myr. Right panel: H_2 mass fractions at the center of halo 073 500 pc from 25, 40, 60 and 80 $M_\odot$ stars from zero to 10 Myr.
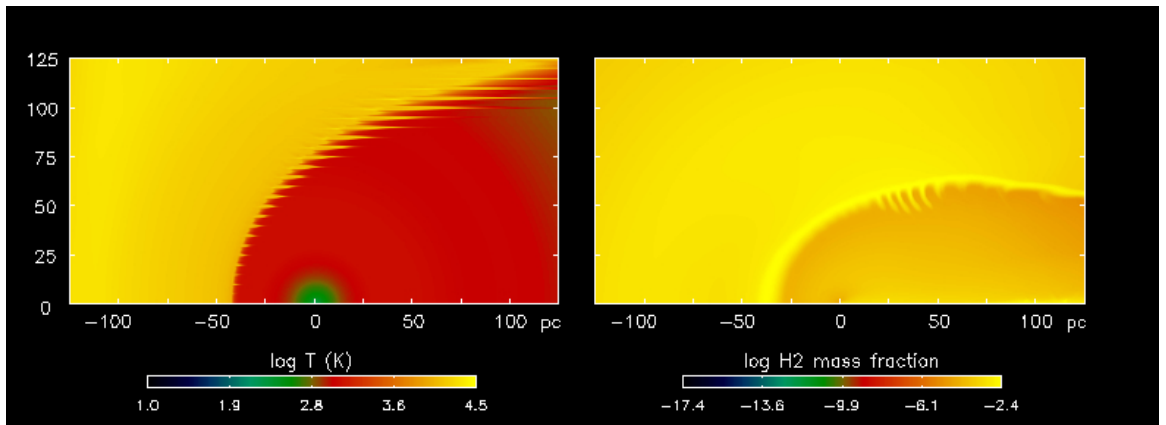
Figure 3.7 Temperatures at 600 kyr (left) and H_2 mass fractions at 10 Myr (right) in halo 073 ($n_c = 1596$ cm^{-3}) 150 pc from a 25 $M_\odot$ star.
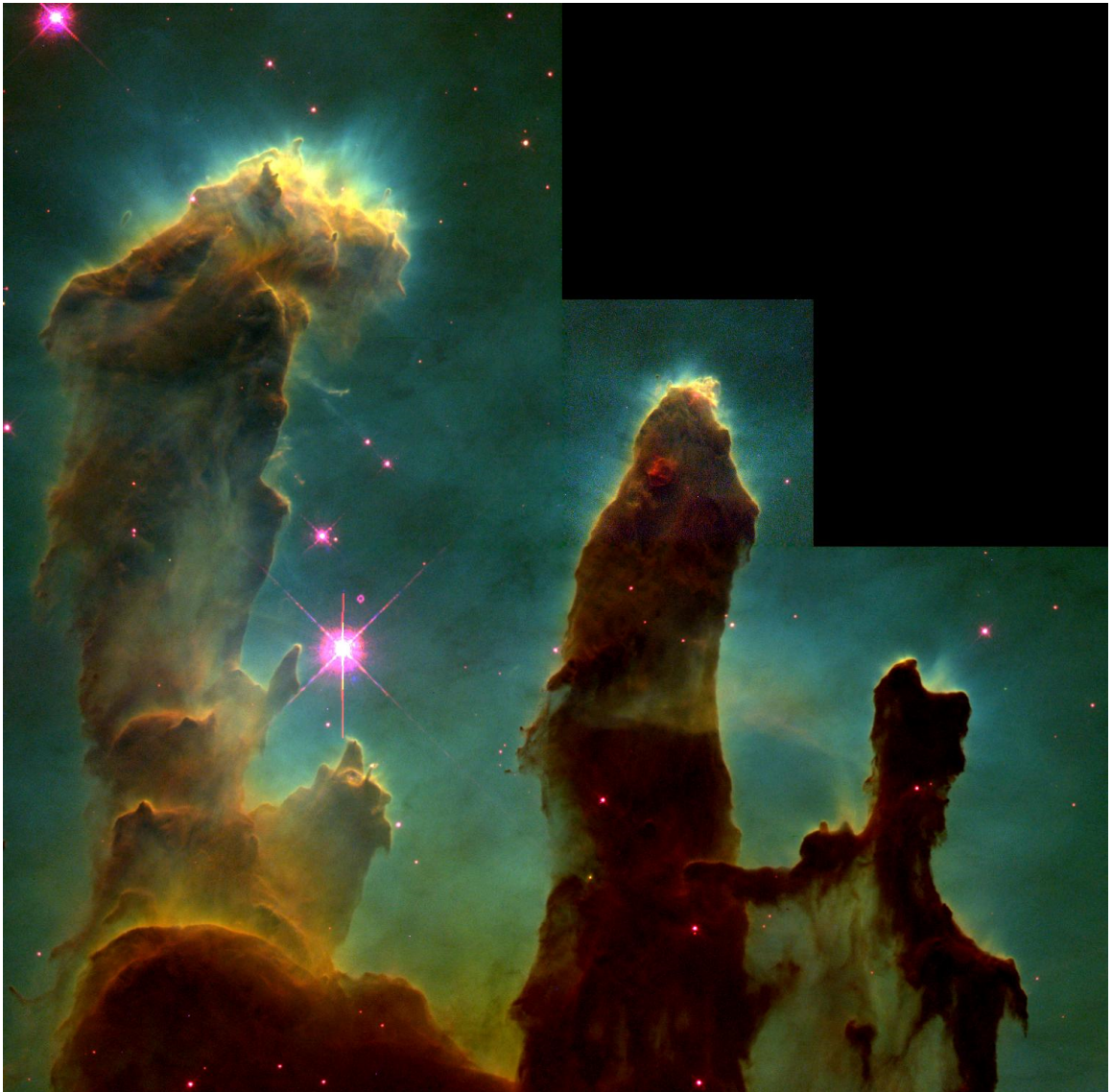
Figure 3.8 The Pillars of Creation in the Orion Nebula are thought to be formed but the same phenomena exhibited in our models.

Chapter 4

Conclusion

We find that 25 - 120 $M_\odot$ primordial stars are relatively uniform in their effect on new star formation within clusters of small halos at high redshifts, before the rise of global LW backgrounds. The evolution in spectral profile from 25 - 120 $M_\odot$ has no impact on the formation of stars in nearby halos, which allows its removal from the parameter space of local radiative feedback. The empirical fits we have devised mark the threshold for star formation in satellite halos as a function of central baryon density, proximity to the star, and neighbor star mass. Although the halo in our study is the just the least massive one found to form a star in previous AMR simulations, our results can be used as upper limits to feedback in more massive halos. Our results imply that future surveys of local feedback with more massive halos can be accomplished with fewer stars, since outcomes for halo photoevaporation above and below the belt in n_c and radius in which there is variability is relatively uniform from 25 - 80 $M_\odot$.

Radiative and kinetic feedback between minihalos is key to many processes in early cosmological structure formation, such as primordial SNe event rates [47], especially those that account for cluster bias [48], the rise of the first stellar populations, the

assembly of primeval galaxies, and the evolution of metagalactic LW backgrounds. Our analytical fits enable feedback estimates for a representative cut of Population III stars in analytical models of these early processes. They can also be used in numerical simulations, especially those performed in large cosmological boxes capable of resolving minihalo clustering but not of capturing halo photoevaporation.

Local radiative feedback at slightly lower redshifts is different due to the presence of LW backgrounds from primordial stars, which until recently has been thought to be quite destructive to new star formation mediated by H_2 cooling in halos [49, 50]. However, recent, more detailed simulations reveal that star formation in cosmological halos is postponed rather than prevented in LW backgrounds, even large ones that are consistent with a fully reionized universe [28, 31]. Whalen et al. [31] found that a halo that formed a star at 5×10^5 $M_\odot$ in the absence of a photodissociative background still formed one by H_2 cooling 50 Myr later after it grew by mergers and accretion to 5×10^6 $M_\odot$ in a uniform LW field of 1 J_{21} ($= 10^{-21}$ erg cm^{-2} Hz^{-1} str^{-1} s^{-1}), that of a fully-ionized universe. Other halos in its vicinity also grew to larger masses, even though cooling and collapse of baryons were temporarily stalled in them. Thus, at lower redshifts local UV feedback still begins when one star irradiates neighbor halos. In contrast to the first generation, LW backgrounds may continue to suppress star formation in photoevaporated halos after the death of the star by slowing the formation of H_2 in the relic H II region, the remnant I-front shock, and the halo core.

However, this effect may have been overestimated in previous analyses. Consider the morphology and large densities and H_2 fractions in the relic H II region at 10 Myr in the right panel of Figure 3.7. Similar H_2 fractions would likely persist in the recombining H II region even in large LW backgrounds because the very high electron fractions there restore it so quickly via the H$^-$ channel. This is especially true in the high densities of the I-front shock remnant, that can be seen to envelope the core in

Figure 3.7. Enough molecular hydrogen could be catalyzed in the envelope to expel the LW background from its interior, allowing H_2 to reform at the center of the halo, cool it, and form a star. Thus, photoevaporation may actually free satellite halos to form stars that were previously suppressed by the background. This, together with our current study, suggests that star formation in cosmological halos at lower redshift was much more robust than is often supposed. Numerical models are now being developed to investigate the survival of molecular hydrogen, and therefore new star formation, in evaporated halos for a range LW backgrounds.

The effect of photoevaporation on the final mass of any star that does form in the halo is not yet well understood, but initial estimates by Susa et al. [51] suggest that it will be smaller than in undisturbed halos. They find that outflows and shock disruption in the core lower central accretion rates, and by extrapolating these rates from early stages of collapse out to Kelvin-Helmholtz contraction time scales, they conclude that the final star will be 25 - 50 $M_\odot$. This mass scale is similar to those on which Pop III.2 stars form due to HD cooling in relic H II regions [52]. HD is important because it can cool primordial H II regions down to the CMB temperature and lower the mass scales on which they fragment. However, we do not include it in our models because it forms primarily in the relic ionized gas surrounding the halo core, not in the core itself.

Although our study is a significant extension to our earlier survey of local radiative feedback, additional feedback channels remain to be properly investigated. If the death of the star results in a black hole, accretion would expose nearby halos to its soft x-ray flux [53, 54], creating significant free electron fractions in them due to secondary ionizations without strongly heating them. This process could enhance their H_2 mass fractions and promote their collapse into new stars. Likewise, the impact of SN ejecta with a halo that has been partially stripped by supersonic flows

could deposit metals into its interior and accelerate its cooling and collapse. These potential avenues of positive feedback on primordial star formation will be the focus of future simulations.

Bibliography

[1] D. Whalen, B. W. O'Shea, J. Smidt, and M. L. Norman, "How the First Stars Regulated Local Star Formation. I. Radiative Feedback," The Astrophysical Journal **679,** 925–941 (2008).

[2] C. L. Bennett *et al.*, "First-Year Wilkinson Microwave Anisotropy Probe (WMAP) Observations: Preliminary Maps and Basic Results," The Astrophysical Journal Supplement Series **148,** 1–27 (2003).

[3] D. N. Spergel *et al.*, "First-Year Wilkinson Microwave Anisotropy Probe (WMAP) Observations: Determination of Cosmological Parameters," The Astrophysical Journal Supplement Series **148,** 175–194 (2003).

[4] D. N. Spergel *et al.*, "Three-Year Wilkinson Microwave Anisotropy Probe (WMAP) Observations: Implications for Cosmology," The Astrophysical Journal Supplement Series **170,** 377–408 (2007).

[5] J. C. Mather *et al.*, "A preliminary measurement of the cosmic microwave background spectrum by the Cosmic Background Explorer (COBE) satellite," Astrophysical Journal, Letters **354,** L37–L40 (1990).

[6] E. L. Wright *et al.*, "Interpretation of the cosmic microwave background radiation anisotropy detected by the COBE Differential Microwave Radiometer," Astrophysical Journal, Letters **396,** L13–L18 (1992).

[7] W. H. Kinney, E. W. Kolb, A. Melchiorri, and A. Riotto, "Inflationary physics from the Wilkinson Microwave Anisotropy Probe," Phys. Rev. D **69,** 103516 (2004).

[8] H. V. Peiris *et al.*, "First-Year Wilkinson Microwave Anisotropy Probe (WMAP) Observations: Implications For Inflation," The Astrophysical Journal Supplement Series **148,** 213–231 (2003).

[9] L. Alabidi and D. H. Lyth, "Inflation models after WMAP year three," Journal of Cosmology and Astro-Particle Physics **8,** 13–+ (2006).

[10] V. Barger, H.-S. Lee, and D. Marfatia, "WMAP and Inflation," Physics Letters B **565,** 33–41 (2003).

[11] L. M. Krauss, "Implications of the Wilkinson Microwave Anisotropy Probe Age Measurement for Stellar Evolution and Dark Energy," Astrophysical Journal, Letters **596,** L1–L3 (2003).

[12] J. L. Tonry *et al.*, "Cosmological Results from High-z Supernovae," Astrophysical Journal **594,** 1–24 (2003).

[13] M. Tegmark *et al.*, "The Three-Dimensional Power Spectrum of Galaxies from the Sloan Digital Sky Survey," Astrophysical Journal **606,** 702–740 (2004).

[14] W. J. Percival *et al.*, "The 2dF Galaxy Redshift Survey: the power spectrum and the matter content of the Universe," Monthly Notices of the RAS **327,** 1297–1306 (2001).

[15] M. Colless *et al.*, "The 2dF Galaxy Redshift Survey: spectra and redshifts," Monthly Notices of the RAS **328,** 1039–1063 (2001).

[16] V. Bromm, P. S. Coppi, and R. B. Larson, "Forming the First Stars in the Universe: The Fragmentation of Primordial Gas," The Astrophysical Journal **527,** L5–L8 (1999).

[17] V. Bromm, A. Ferrara, P. S. Coppi, and R. B. Larson, "The fragmentation of pre-enriched primordial objects," Monthly Notices of the RAS **328,** 969–976 (2001).

[18] T. Abel, G. L. Bryan, and M. L. Norman, "The Formation of the First Star in the Universe," Science **295,** 93–98 (2002).

[19] T. Abel, G. L. Bryan, and M. L. Norman, "The Formation and Fragmentation of Primordial Molecular Clouds," Astrophysical Journal **540,** 39–44 (2000).

[20] F. Nakamura and M. Umemura, "On the Initial Mass Function of Population III Stars," The Astrophysical Journal **548,** 19–32 (2001).

[21] F. Nakamura and M. Umemura, "On the Mass of Population III Stars," The Astrophysical Journal **515,** 239–248 (1999).

[22] B. W. O'Shea and M. L. Norman, "Population III Star Formation in a ΛCDM Universe. I. The Effect of Formation Redshift and Environment on Protostellar Accretion Rate," The Astrophysical Journal **654,** 66–92 (2007).

[23] D. Schaerer, "On the properties of massive Population III stars and metal-free stellar populations," Astronomy and Astrophysics **382,** 28–42 (2002).

[24] M. E. Machacek, G. L. Bryan, and T. Abel, "Simulations of Pregalactic Structure Formation with Radiative Feedback," Astrophysical Journal **548,** 509–521 (2001).

[25] M. E. Machacek, G. L. Bryan, and T. Abel, "Effects of a soft X-ray background on structure formation at high redshift," Monthly Notices of the RAS **338,** 273–286 (2003).

[26] A. Mesinger, G. L. Bryan, and Z. Haiman, "Ultraviolet Radiative Feedback on High-Redshift Protogalaxies," The Astrophysical Journal **648,** 835–851 (2006).

[27] B. W. O'Shea, T. Abel, D. Whalen, and M. L. Norman, "Forming a Primordial Star in a Relic H II Region," Astrophysical Journal, Letters **628,** L5–L8 (2005).

[28] B. W. O'Shea and M. L. Norman, "Population III Star Formation in a ΛCDM Universe. II. Effects of a Photodissociating Background," The Astrophysical Journal **673,** 14–33 (2008).

[29] M. Ricotti, N. Y. Gnedin, and J. M. Shull, "The Fate of the First Galaxies. I. Self-consistent Cosmological Simulations with Radiative Transfer," Astrophysical Journal **575,** 33–48 (2002).

[30] A. Mesinger, G. L. Bryan, and Z. Haiman, "Radiative Feedback in Relic HII Regions at High-Redshift," ArXiv e-prints (2008).

[31] J. H. Wise and T. Abel, "Suppression of H_2 Cooling in the Ultraviolet Background," The Astrophysical Journal **671,** 1559–1567 (2007).

[32] H. Susa and M. Umemura, "Secondary Star Formation in a Population III Object," Astrophysical Journal, Letters **645,** L93–L96 (2006).

[33] K. Ahn and P. R. Shapiro, "Does radiative feedback by the first stars promote or prevent second generation star formation?," Monthly Notices of the RAS **375,** 881–908 (2007).

[34] K. Hasegawa, M. Umemura, and H. Susa, "Radiative regulation of Population III star formation," Monthly Notices of the RAS **395,** 1280–1286 (2009).

[35] M. Ricotti and J. M. Shull, "Feedback from Galaxy Formation: Escaping Ionizing Radiation from Galaxies at High Redshift," Astrophysical Journal **542,** 548–558 (2000).

[36] D. Whalen and M. L. Norman, "Ionization Front Instabilities in Primordial H II Regions," The Astrophysical Journal **673,** 664–675 (2008).

[37] D. J. Whalen, Ph.D. thesis, University of Illinois at Urbana-Champaign, 2006.

[38] P. Anninos, Y. Zhang, T. Abel, and M. L. Norman, "Cosmological hydrodynamics with multi-species chemistry and nonequilibrium ionization and cooling," New Astronomy **2,** 209–224 (1997).

[39] T. Abel, P. Anninos, Y. Zhang, and M. L. Norman, "Modeling primordial gas in numerical cosmology," New Astronomy **2,** 181–207 (1997).

[40] H. Kirchoff, "On the Simultaneous Emission and Absorption of Rays," Philosophical Magazine **19,** 193 (1860).

[41] B. W. O'Shea, G. Bryan, J. Bordner, M. L. Norman, T. Abel, R. Harkness, and A. Kritsuk, "Introducing Enzo, an AMR Cosmology Application," ArXiv Astrophysics e-prints (2004).

[42] I. T. Iliev *et al.*, "Cosmological radiative transfer comparison project II. The radiation-hydrodynamic tests.," Monthly Notices of the Royal Astronomical Society .

[43] M. Ricotti, N. Y. Gnedin, and J. M. Shull, "Feedback from Galaxy Formation: Production and Photodissociation of Primordial H_2," Astrophysical Journal **560,** 580–591 (2001).

[44] R. J. R. Williams, "On the instability of D-type ionization fronts.," Monthly Notices of the Royal Astronomical Society **331,** 693706 (2002).

[45] A. Mizuta, J. O. Kane, M. W. Pound, B. A. Remington, D. D. Ryutov, and H. Takabe, "Formation of Pillars at the Boundaries between H II Regions and Molecular Clouds," Astrophysical Journal**647,** 1151–1158 (2006).

[46] E. T. Vishniac, "The dynamic and gravitational instabilities of spherical shocks," Astrophysical Journal**274,** 152–167 (1983).

[47] J. H. Wise and T. Abel, "The Number of Supernovae from Primordial Stars in the Universe," Astrophysical Journal**629,** 615–624 (2005).

[48] M. A. MacIntyre, F. Santoro, and P. A. Thomas, "On the population of primordial star clusters in the presence of ultraviolet background radiation," Monthly Notices of the Royal Astronomical Society **368,** 1301 – 1310 (2006).

[49] Z. Haiman, M. J. Rees, and A. Loeb, "Destruction of Molecular Hydrogen during Cosmological Reionization," The Astrophysical Journal **476,** 458 (1997).

[50] N. Yoshida, T. Abel, L. Hernquist, and N. Sugiyama, "Simulations of Early Structure Formation: Primordial Gas Clouds," Astrophysical Journal**592,** 645–663 (2003).

[51] H. Susa, M. Umemura, and K. Hasegawa, "Formation Criteria and the Mass of Secondary Population III Stars," Astrophysical Journal**702,** 480–488 (2009).

[52] N. Yoshida, P. S. Oh, T. Kitayama, L. Hernquist, and N. Sugiyama, "Early Cosmological H II/He III Regions and Their Impact on Second-Generation Star Formation," Astrophysical Journal**663,** 687–707 (2007).

[53] M. E. Machacek, G. L. Bryan, and T. Abel, "Effects of a soft X-ray background on structure formation at high redshift," Monthly Notices of the Royal Astronomical Society **338,** 273 – 286 (2003).

[54] M. A. Alvarez, J. H. Wise, and T. Abel, "Accretion onto the First Stellar-Mass Black Holes," Astrophysical Journal Letters **701,** L133–L137 (2009).